

Interpretation value of diffractions and sub-specular reflections – applications on the Zhao Dong field

Michael Pelissier¹, Tijmen Jan Moser^{2*}, Changhua Yu³, Jing Lang³, Ioan Sturzu⁴ and Alexander Mihai Popovici⁴

Abstract

We provide an overview of integrated pre-stack depth migration and diffraction imaging for the Zhao Dong field, Bohai Bay, China. This field is highly compartmentalized by complex faulting and further characterized by channel systems, fractures and volcanic features. The objective of the diffraction imaging is to better define these small-scale features. Tools to facilitate interpretation include displays with pre-stack depth migration and diffraction images overlain in different colour scales, as well as a weighted blending of them into a single volume. An important concept is that of the sub-specular reflection, which is obtained alongside the pure diffraction image by applying ultra-weak specular tapering. Tuning properties of elementary diffractor images together with sub-specular reflectors provide a decisive uplift of diffraction imaging for the interpreter.

Introduction

Zhao Dong is a mature oil field located in Bohai Bay, China. The Bohai Bay basin is an inter-continental rift basin (Zaisheng, Zhu and Zheng, 1994). The tectonics and seismic stratigraphy of the Zhao Dong field are detailed by Castellanos (2007). The main reservoirs are in the Neogene and these have excellent reservoir properties. The Pliocene Minghausen formation consists of generally isolated meandering channels set in floodplain facies. The Miocene Guantao formation consists of braided and amalgamated fluvial systems. The Paleogene reservoirs are of lesser reservoir quality, and include lacustrine and deltaic in addition to fluvial sands. The Mesozoic reservoirs consisting of lacustrine and fluvial sands, have generally poor matrix porosities. For these reservoirs fracture porosity is important for production. The Zhao Dong field is subdivided into two main fault blocks and several large sub-blocks. As noted in Castellanos (2007), the oblique-slip reactivation of the main fault has resulted in a negative flower structure. A large number of smaller fault blocks lie within this structure.

Because of its complexity, Zhao Dong is classified as a marginal field. However, production has typically exceeded expectations as increasingly sophisticated field development methods have been applied to produce smaller pools with thinner sands and infill previous drilling in the larger pools. Whereas the early field development used multi-zone producers, the later development has been with horizontal producers. Most of the pools have limited aquifer support; a large number of injection wells support reservoir pressures in the various pools.

In order to support the drilling programme, PSDM (pre-stack depth migration) reprocessing and diffraction imaging were carried out in 2014/2015. The PSDM reprocessing provided an improved reflection image, which in turn provided a better baseline product for localized spectral whitening to support well planning for specific pools. The diffraction image provided improved definition of faults and fractures, as well as stratigraphy and volcanic features. To customize the PSDM and diffraction imaging results for the interpretation objectives, workflows were developed for integrating the results in the interpretation environment.

Seismic diffractions are the response of subsurface discontinuities (Klem-Musatov et al., 2016a, b). Unlike reflections, which follow Snell's law and are subject to illumination constraints, edge and tip diffractions are generated by line and point sources, without constraints on illumination. In addition, diffractions allow high-resolution imaging of structural details not normally visible on regular (PSDM) images. This makes them a good candidate to image the faults, fractures, channel systems and volcanic features present in Zhao Dong. The workflow for diffraction imaging used here is similar to the one presented in Moser and Howard (2008). A key ingredient in the diffraction imaging is the specular tapering (Sturzu et al., 2013), which provides diffraction images with a different degree of structural detail. The specular taper is specified by a percentage: the closer to 100%, the weaker the taper, and the closer the resulting diffraction image resembles the original regular PSDM. Following Pelissier et al. (2015), in

¹ Integrated Geoscience Solutions, formerly Dagang Zhaodong Oil Company of PetroChina | ² Moser Geophysical Services

³ PetroChina | ⁴ Z-Terra Inc

* Corresponding author, E-mail: t.j.moser@mgeoph.com

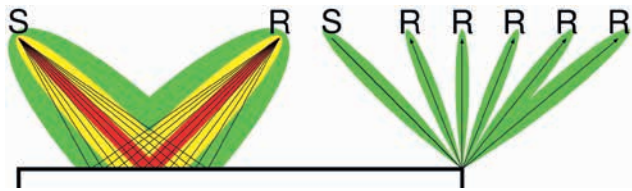


Figure 1 Reflection and diffraction Fresnel zones for given source/receivers (S/R). Diffraction imaging suppressed specular reflection (red) and enhanced non-specular diffraction (green), with sub-specular reflection (yellow) in between.

this paper we study the interpretation impact of ultra-weak taper diffraction images, which have subtle but essential differences compared with the regular PSDM.

Diffraction imaging

In our diffraction imaging workflow, we produce a pre-stack data set that is sorted by specularity instead of offset (Sturzu et al., 2013, 2014). Therefore, the specularity gather samples a continuum of a wavefield that grades between reflections and diffractions. Diffraction images are obtained by tapering the specularity gathers at a judiciously chosen value and stacking them. As we increase the specularity taper, we are removing the reflection contribution from the inner portion of the Fresnel zone (the red zone in Figure 1); this is the same as removing the leading edge of the reflected wavefield. The residual of the taper consists of pure diffractions (green in Figure 1) and remnant reflections (yellow), which are outside the pure specular ray but still contribute constructively to a remnant reflection image. We refer to the remnant reflections as *sub-specular reflections*. They can be easily filtered out from the final diffraction image, but in this paper we make a case for their interpretation value.

Sub-specular reflection

The effect of specularity suppression is illustrated in the conceptual images of Figure 2. The pure specular reflection corresponds to the main reflector (red, Figure 2a). Removing it by a weak taper results in a combination of a diffraction image and sub-specular

reflection image (green and yellow, Figure 2b), a strong specularity taper leads to a pure diffraction image (green, Figure 2c).

A concept diagram of the image as a function of specularity is given in Figure 3a. Here we can see that as we progressively remove the leading edge, the image defined by the new envelope of constructive interference will move up towards the acquisition before eventually dissolving. Therefore, as we increase the specularity taper, the remnant reflectors will progressively move up to shallower depths. The response for a synthetic model of a faulted reflector as a function of the specularity taper and depth is shown in Figure 3b. An important feature observed in this figure is that the diffraction points are fixed. Unlike the sub-specular reflections, they do not move up towards the acquisition as the taper increases. In this paper we stress the interpretation value of the combined diffraction image and imaged sub-specular reflections for ultra-weak specularity tapers.

Diffraction imaging and tuning

As an improved definition of faulting is the main objective of the Zhao Dong diffraction imaging, it is instructive to review the diffraction image response to faulting. The edge diffraction is the elementary building block of the fault response. In Figure 4, we show the migration of a model with three faulted reflectors. The key property of the imaged edge diffraction is the polarity reversal. This is illustrated by the isolated edge diffraction image (Figure 4a). The edge diffraction image consists of several amplitude maxima and minima which are symmetrically grouped about the exact edge point of the reflector; we refer to this as the *diffraction quadrupole image* (as in the simplest case there are four poles with pairwise opposite polarities). The imaged diffraction beyond the end of the reflector has the same polarity as that of the reflector. There is a zero crossing at the edge, and before the edge, the polarity is opposite to the reflector polarity. Because of this, in the case of a (sub)vertical fault, the polarities of the diffraction images associated with the upthrown and downthrown sides are opposite.

As illustrated by Landa and Gurevich (1998) on a synthetic model, we can expect that the interference pattern of diffractions



Figure 2 Diffraction imaging on a simple reflector model. Specular reflection energy (red) is suppressed, pure diffraction (green) is preserved. Sub-specular reflectivity (yellow) forms a transition between the two.

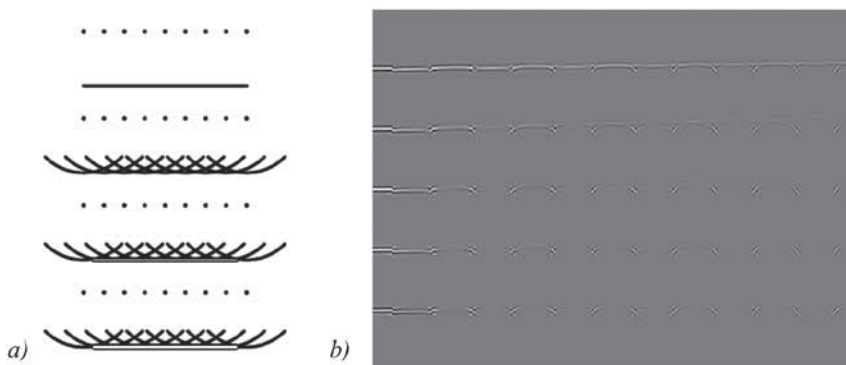


Figure 3 (a) Removal of specular reflection (dots denote coincident source/receiver points); (b) diffraction image as function of depth and specularity taper (varying from no taper at the left to a very strong one at the right).

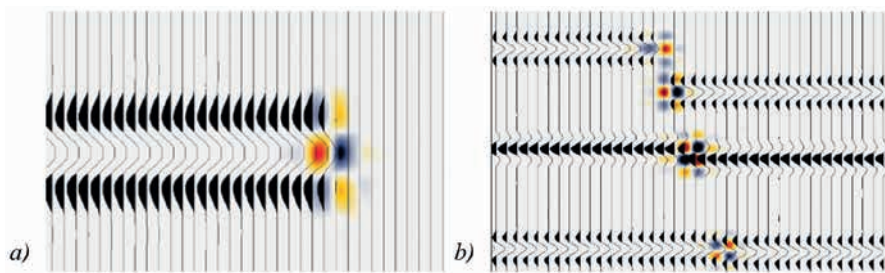


Figure 4 Building blocks of diffraction image. (a) zoom on isolated edge diffractor image (colour) and associated regular migration image (wiggles); (b) composite diffractor images showing tuning as fault throw decreases.

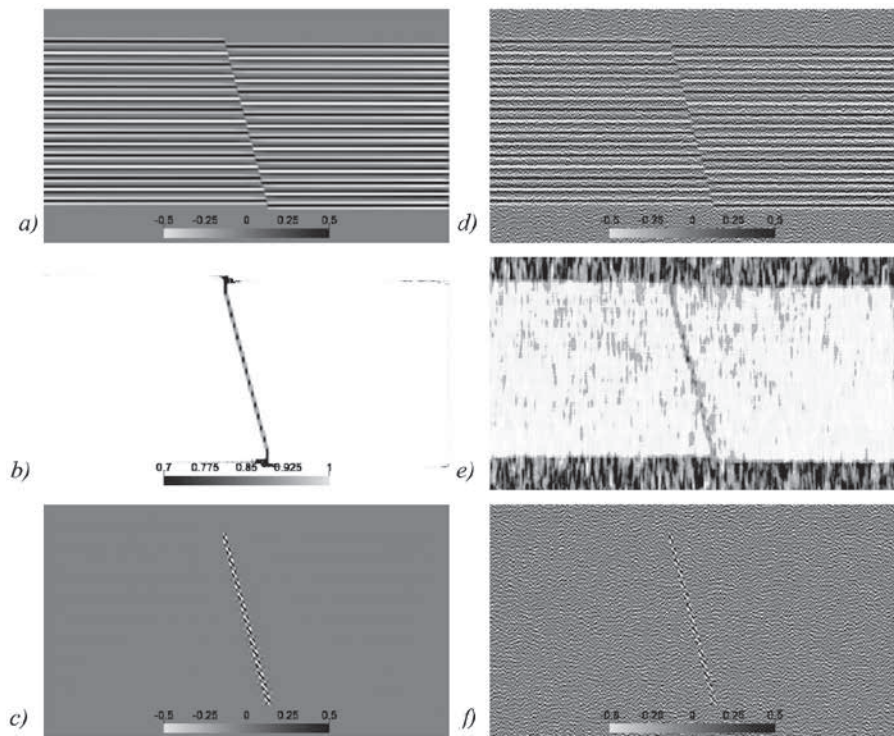


Figure 5 Comparison of PSDM, coherence and diffraction image (top to bottom) on noise-free and noisy data (left and right). Note amplitude and structural fault information conveyed by diffraction image, even with enhanced noise level.

will provide information to aid the interpretation process. This interference applies to both raw and imaged diffractions. From Figure 4b it is clear that, if the throw is small enough, the imaged diffractions interfere in the same way as the reflections for a thin bed problem, resulting in the behaviour detailed in the classic paper by Widess (1978). Below tuning, the imaged diffraction events will be displaced vertically, just as a very thin layer has an apparent peak/trough thickness greater than its actual thickness. For the diffractions, the main amplitudes will be shifted up from the termination of the reflector on the upthrown side, and down from the reflector termination on the downthrown side. As the throw vanishes, so does the amplitude of the composite diffraction.

Relation to coherence

A diffraction image is fundamentally different from most seismic attributes as it provides a physical seismic image with amplitude, phase and kinematic properties. To illustrate this, Figure 5 offers a comparison of coherence and diffraction imaging for a densely layered model with alternating reflection polarities, cut by a single dipping fault. In the noise-free case, the coherence detects the reflector terminations but smears them out at the top and bottom. The noise-free diffraction image correctly positions the individual reflector terminations (edge diffractors). Because of the composite quadrupole character of the diffraction image, the

reflector amplitude and polarity, as well as the fault dip can be estimated. The diffraction image can therefore be interpreted in both a kinematic and dynamic sense. After adding a high noise level (SNR=3) to both the PSDM and diffraction imaging, and subsequently deriving coherence from the PSDM, we see that the diffraction image still reveals the kinematic and dynamic information, but that the coherence is blurred and loses resolution with regards to the individual reflector terminations. The diffraction image is relatively robust to noise since it is constructed pre-stack and pre-migration, rather than post-stack/migration.

Integrated visualization of methods for PSDM and diffraction imaging

In interpreting the Zhao Dong PSDM and diffraction imaging results, we have used several visualization methods. These include semi-transparent overlays, the use of coherence as a template for blending the PSDM and diffraction images, and suites of diffraction images with mild specularly tapers. These methods are especially useful for the interpretation of seismic sections.

Semi-transparent overlays and blending

The simplest method for integrating the PSDM and diffraction images is to use opacity control in the interpretation software to overlay a semi-transparent diffraction image display on the

PSDM display. In this case, we make the low amplitude areas of the diffraction image completely transparent. The semi-transparent overlays are also useful for working with coherence in section view; in this case, the opacity is set to make the high values of coherence transparent. In both cases, the use of overlays requires the user to make a careful choice of the colour bar and opacity settings. The overlay method is especially useful for reconnaissance of the main features in the diffraction image. A disadvantage of this method is that the display capabilities and controls vary between interpretation systems.

A comparison of a coherence overlay with a diffraction overlay is shown in Figures 6a and 6b, respectively. Here we can see that both images identify various small faults, but that the diffraction imaging overlay provides higher resolution. This is because the diffraction image is a wavefield, whereas coherence requires averaging over temporal and spatial windows.

For the Zhao Dong interpretation, we piloted a blending method using coherence to combine seismic reflections and diffractions in a single volume. As Lin et al. (2014) pointed out, coherence anomalies can be due to geological reasons, such as sharp discontinuities or karst features, lower reflectivity associated with imaging problems or random noise. However, diffraction energy is at a maximum for geological features such as faults or karst. Therefore, in areas of low coherence, we can substitute the diffraction image for the reflection image to produce a blended volume. We can use a single coherency cutoff below which the diffraction image is substituted for the diffracting image, or a coherence range to provide a transition over which the diffraction image is gradually blended in. The PSDM is shown in Figure 6c, and the same section with the PSDM replaced by a diffraction image for coherence values above 0.9 is shown in Figure 6d.

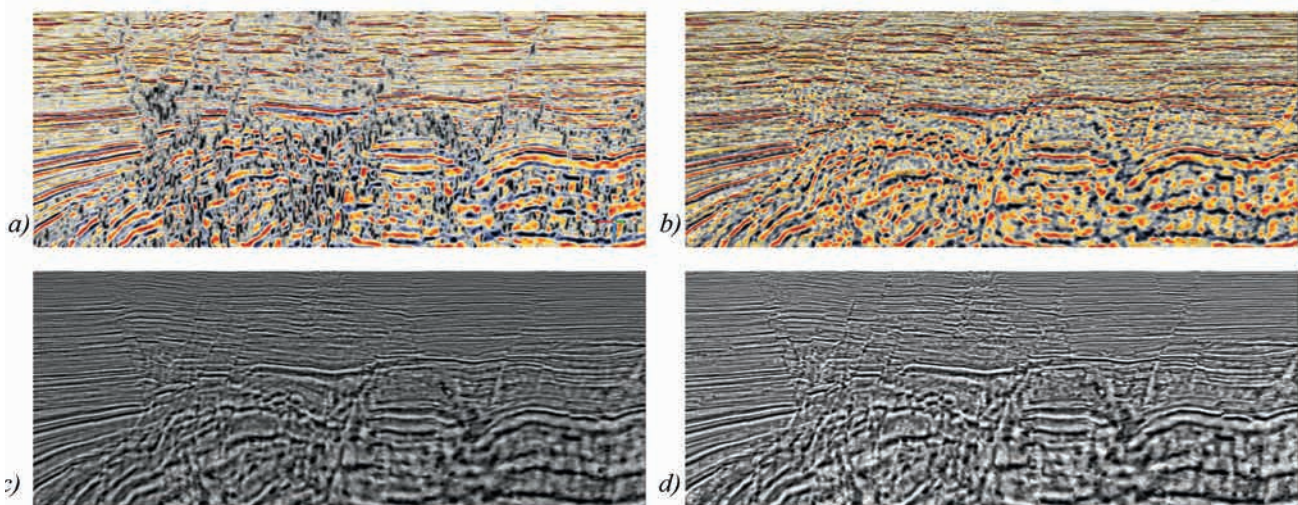


Figure 6 PSDM with (a) coherence and (b) diffraction image overlay; (c) PSDM; (d) PSDM with blended diffraction image.

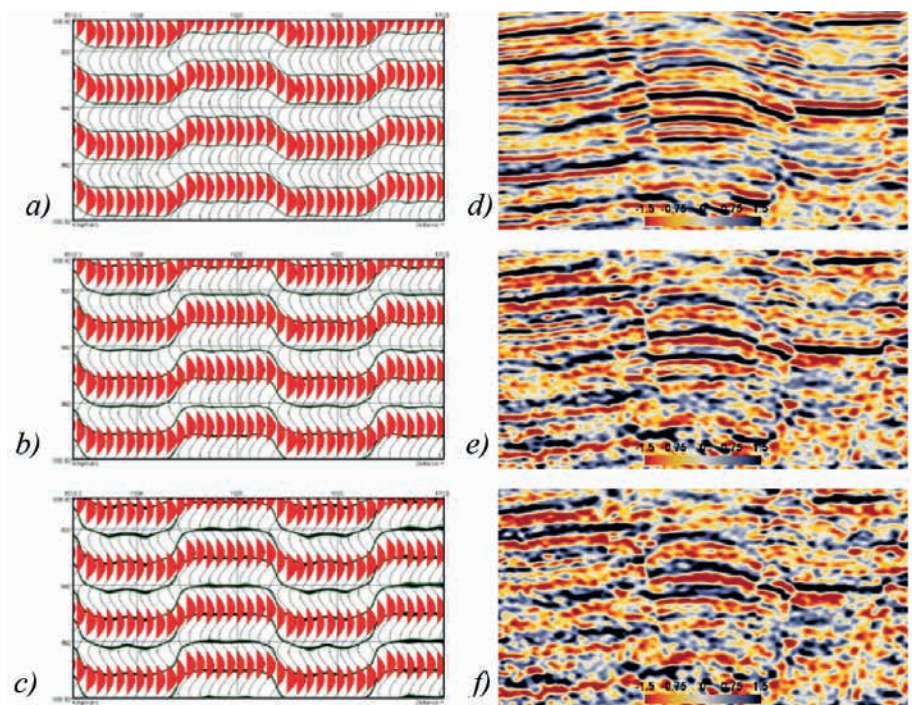


Figure 7 Left: PSDM (red wiggles) with zero crossings of PSDM (a) and diffraction images with increasing taper (b) 99% and (c) 98% overlain. Note the fault throw amplification by increasing taper. Right: comparable effect in Zhao Dong PSDM (d) and diffraction images with increasing taper (e) 99.5% and (f) 99.0%.

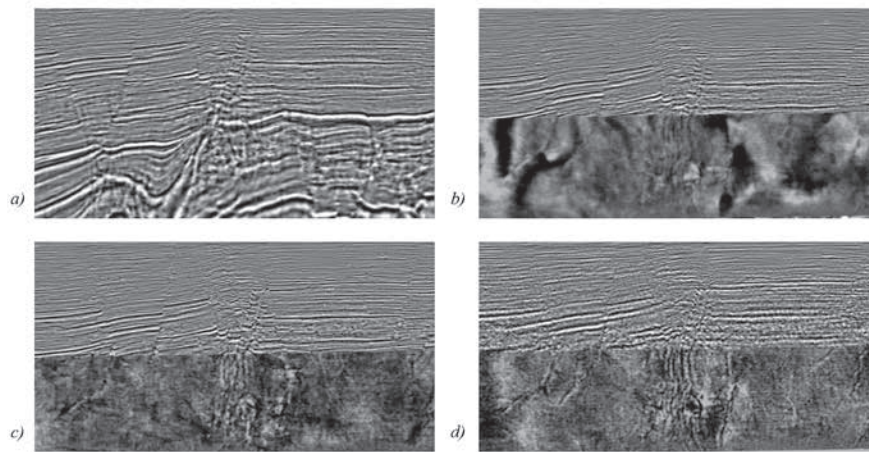


Figure 8 Flower structure. (a) PSDM section; (b) PSDM chair section (vertical section and depth slice); (c) chair section: vertical section DI 99% blended with PSDM, depth slice pure DI 99%; (d) chair section pure DI 98%.

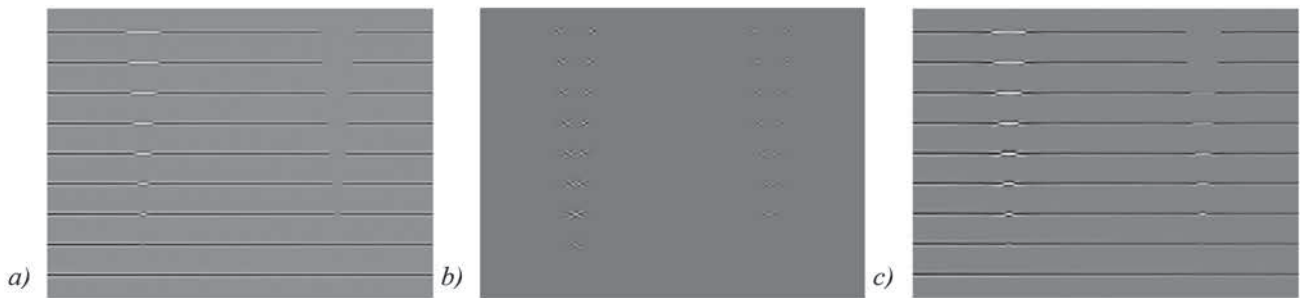


Figure 9 Channel model imaging. (a) regular PSDM; (b) pure diffraction image; (c) diffraction image at ultra-weak taper (99.90%).

Sub-specular reflections and diffractions

The blending method has a resolution limit since small faults may be bypassed by the coherence template. Furthermore, areas of low coherence due to poor signal/noise on the PSDM can introduce artifacts in the blending process. To exploit the finer detail in the diffraction imaging, we used suites of diffraction images with mild tapers. We refer to such images as sub-specular. The tapers are mild enough so that the remnant reflections for key geological markers can be still be recognized, despite their upward shift and lower frequency. In analogy to 3D pre-stack interpretation for the interpretation of reflections, the suites of sub-specular images provide an additional level of detail regarding sub-surface discontinuity. As noted above, the application of the various specularity tapers represents a continuum between reflection and diffraction. The Zhao Dong imaging shows that the relation between sub-specular reflectors and diffraction points as a function of the specularity taper is highly sensitive to faulting. In particular, the sub-specular images show an amplification of throw on small faults, thus aiding in the detectability of faults. Based on this observation, we used seismic modelling and imaging to investigate the sub-specular response of closely spaced faults having a small throw. The results for fault blocks with a width of 50 m, with vertical faults having a throw of 5m is shown in Figure 7 (left). Here we have overlain the zero crossings of the sub-specular images on the PSDM. Note that as the taper increases, the zero crossings diverge significantly, increasing the apparent throw. These sub-specular reflections are anchored to the fixed diffraction points, which are below tuning for small throws, resulting in the apparent throw amplification. This same throw amplification effect is observed on the sub-specular real data images shown in

Figure 7 (right). We have found that cycling through the suite of sub-specular images is especially useful in detecting small scale faults. Since the diffraction points remain fixed, the interpreter can observe the remnant reflectors moving upwards along fault planes as the specularity decreases.

Diffraction imaging of main structural features

The main structural features of Zhao Dong are illustrated in Figure 8. The cross-section view of the PSDM and sub-specular images shows the two main fault blocks of Zhao Dong, which are lying on either side of a negative flower structure. The tilted fault blocks form the tapping mechanism for a large number of hydrocarbon pools at various stratigraphic levels. Producing pools are also located within the smaller blocks within the flower structure. The diffraction imaging provides an additional level of fault definition over the PSDM. In the interpretation of any given hydrocarbon pool, the fault definition can be further investigated using the sub-specular images.

Stratigraphic diffraction imaging

Stratigraphic definition is a critical factor in the development of the fluvial sand reservoirs in Zhao Dong's Minghausen and Guanto Formations. Whereas most of the pools are structural, with a combination of fault and dip closure, a number of pools include stratigraphic pinchouts. Moreover, the drilling of a horizontal producer requires high accuracy in sand body definition. Diffraction imaging offers improved resolution of channel and intra-channel edges since these are associated with seismic diffractions. Fomel, Landa and Taner et al. (2007) demonstrated the resolution power of diffraction imaging using a synthetic 3D model of a meandering channel system. Here we use a synthetic

model based on Zavalishin (1982), who used a step function in reflectivity to represent diffraction at a deposit edge. In the concept model shown in Figure 9, we replace segments of reflecting boundaries with a different reflectivity. In the sequence in the left of the model, we use a reflectivity with an equal magnitude and reverse polarity. This represents a maximum lateral contrast in the edge diffractions. Given the opposite polarities, the edge diffractors will interfere constructively, providing a strong amplitude in the diffraction image of the edge of the channel. As the channel width decreases, lateral tuning of the diffractors from either edge further assists the detectability of the channel even for very mild specularity tapers. On the right hand side of the model in Figure 9a, the channel is represented by gaps of zero

reflectivity. Diffractions occur at the channel edges, but there is no interference effect. However, the sub-specular reflections produce an anomaly over the channel. Unlike the specular rays, the non-specular rays from the host rock reflector form an event positioned above the channel.

From the model results, we can better appreciate the diffraction imaging of a Zhao Dong channel feature seen in the horizon amplitudes displayed in Figure 10. With increasing specularity taper, the main channel splits into two segments. This additional resolution is significant for horizontal well planning. In Figure 10 we also see very narrow channel features come into focus. This effect, and the splitting of the main channel, are consistent with the concept model results. The stratigraphic diffraction imaging

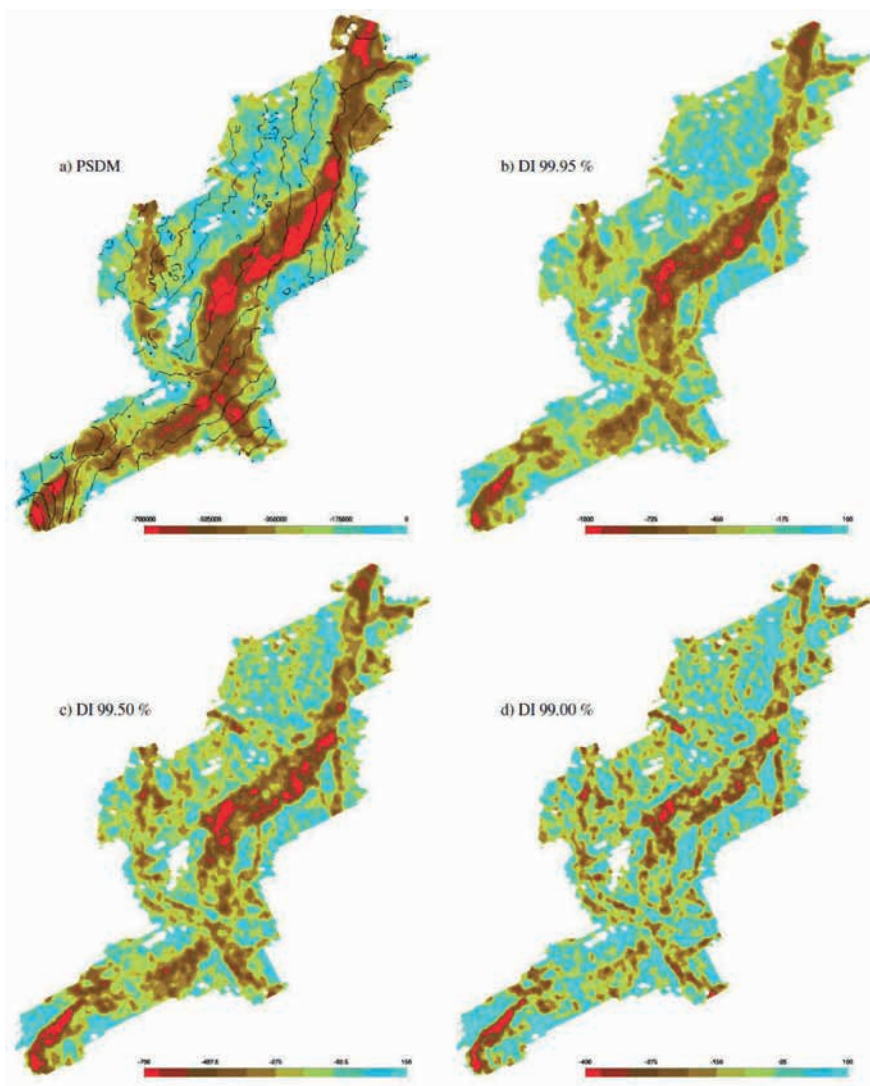


Figure 10 Channel images. Regular PSDM (a, with 10 m depth contours) and diffraction images with different specularity tapers, as indicated by percentages (b-d).

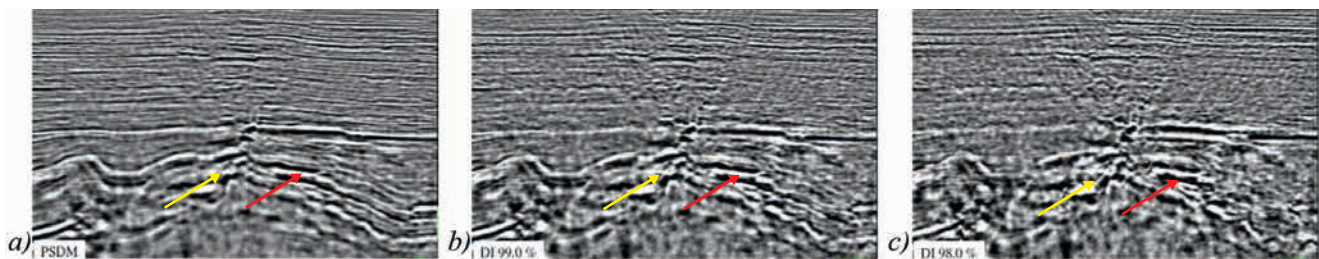


Figure 11 PSDM and diffraction images at 99 % and 98 % of a crossline, showing densely faulted/fractured Mesozoic reservoir (yellow) and continuous reflector (red).

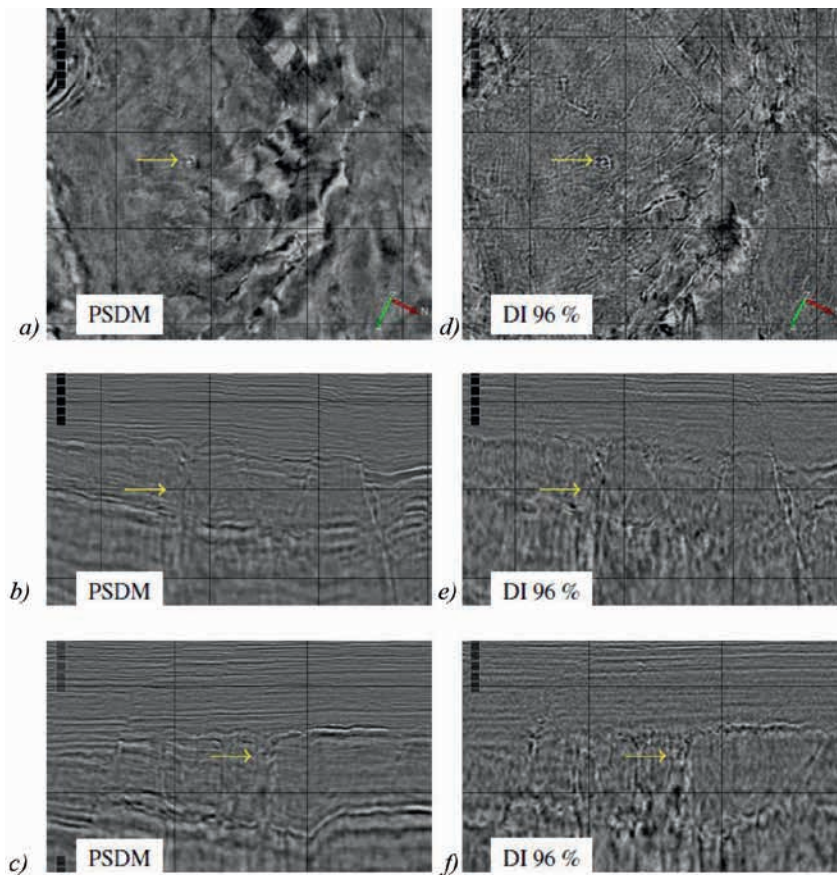


Figure 12 P Volcanic pipe. Volcanic pipe, indicated by yellow arrow. Top to bottom: depth slice, in- and crossline section. Left: PSDM, right: DI 96%.

brings out the signature of a braided system, which is less obvious on the PSDM.

Small-scale faults and fractures

The throw magnification for small faults has important implications for the development of the Mesozoic reservoirs in Zhao Dong. The production of these deeper and structurally more complex reservoirs is dependent on fracture porosity, which in turn is likely to be associated with areas of very dense small-scale faulting. This is illustrated in Figure 11. Areas of dense faulting come into focus for very small increases in the specularly taper. This phenomenon was first observed on the diffraction imaging of the Eagle Ford shale (Sturzu et al., 2014).

Volcanics

Bohai Bay features a number of reservoirs in volcanic rocks, as detailed by Chunshuang, Dewu and Weining (2012) as well as Zou (2013). The volcanic activity which occurred in the various phased of rifting are documented by Liu et. al (2012). Although volcanic reservoirs have not been encountered in Zhao Dong, volcanics are present in the Mesozoic (Castellanos, 2007). The seismic response from vertically aligned objects like volcanic pipes is typically dominated by diffractions, due to their favourable illumination properties (Moser et al., 2016). Diffraction imaging can therefore assist in the identification of volcanic pipes in Zhao Dong and has potential to for wide applicability to the extensive volcanics present in Bohai Bay.

An example of a possible volcanic pipe is shown in Figure 12. The pipe shows up as a circular feature on depth slices. On the

PSDM sections, this shows up as a vertical zone with very poor reflectivity which could easily be interpreted as noise. On the diffraction images, the definition of the pipe is much clearer; a low S/N area on the PSDM is replaced by a relatively higher S/N area on the diffraction image.

Conclusions and recommendations

Structural and stratigraphic diffraction imaging prove to be effective in resolving small-scale details in a range of interpretation environments, in Zhao Dong and similar fields. The structural diffraction imaging enhances the details of the complex faulting at both the fault block and reservoir scales. Stratigraphic diffraction imaging is able to resolve the internal geometries of channel systems. The volcanic features in Zhao Dong are also better resolved by diffraction imaging. The combination of structural and stratigraphic diffraction imaging has the potential to benefit the field development of Zhao Dong and other Bohai Bay fields.

The improved resolution is provided by the wavefield diffracted from sub-wavelength subsurface features. From first principles, this method has greater resolving power than attributes derived from post-processing of the PSDM. Sub-specular reflections obtained from ultra-weak specularly tapers provide an important auxiliary interpretation tool. Kinematic information provided by focusing and tuning properties, as well as dynamic information of the pure diffraction and sub-specular reflection images, provide a wealth of previously unseen interpretation detail. Visualization tools, such as overlay displays and blending of regular and diffraction images and suites of diffraction images with decreasing taper, help to make this detail visible.

Acknowledgements

We would like to thank the Dagang Zhaodong Oil Company of PetroChina for permission to show the Bohai Bay seismic data.

References

Castellanos, H.A. [2007]. *Sequence Stratigraphy and Tectonics of the Guantao and Minghuazhen Formations, Zhao Dong Field, Bohai Bay, Eastern China*. PhD thesis, University of Texas.

Chunshuang, J., Dewu, Q. and Weining, D. [2012]. Meso-Cenozoic volcanic rock distribution and reservoir characteristics in the Bohai Bay Basin. *Oil & Gas Geology*, **33**, 19-29.

Fomel, S., Landa, E. and Taner, M.T. [2007]. Poststack velocity analysis by separation and imaging of seismic diffractions. *Geophysics*, **72**, U89-U94.

Klem-Musatov, K., Hoerber, H.C., Moser, T.J. and Pelissier, M.A. [2016a]. *Classical and Modern Diffraction Theory*, Geophysics Reprint Series No. 29.

Klem-Musatov, K., Hoerber, H.C., Moser, T.J. and Pelissier, M.A. [2016b]. *Seismic Diffraction*, Geophysics Reprint Series No. 30.

Landa, E. and Gurevich, B. [1998]. Interference pattern as a means of fault detection. *The Leading Edge*, **17** (6), 752-757.

Lin, T., Ha, T., Marfurt, K.J. and Deal, K.L. [2016]. Quantifying the significance of coherence anomalies. *Interpretation*, **4** (2), T205-T213.

Liu, J., Wang, P., Zhang, Y., Bian, W., Huang, Y., Tang, H. and Chen, X. [2012]. *Volcanic Rock-Hosted Natural Hydrocarbon Resources: A Review*. In: Nemeth, K. (Ed.) *Updates in Volcanology - New Advances*

in *Understanding Volcanic Systems*, Publisher InTech.

Moser, T.J. and Howard, C.B. [2008]. Diffraction imaging in depth. *Geophysical Prospecting*, **56**, 627-641.

Moser, T.J., Arntsen, B., Johansen, S., Raknes, E.B. and Sangesland, S. [2016]. Seismic Diffraction Response from Boreholes. *78th EAGE Conference and Exhibition*, Expanded Abstracts.

Pelissier, M.A., Moser, T.J., Jing, L., de Groot, P., Sirazhiev, A., Sturzu, I. and Popovici, A.M. [2015]. Diffraction Imaging of the Zhao Dong Field, Bohai Bay, China. *77th EAGE Conference and Exhibition*, Expanded Abstracts.

Sturzu, I., Popovici, A.M., Tanushev, N., Musat, I., Pelissier, M.A. and Moser, T.J. [2013]. Specularity Gathers for Diffraction Imaging. *75th EAGE Conference and Exhibition*, Expanded Abstracts.

Sturzu, I., Popovici, A.M., Pelissier, M.A., Wolak, J.M. and Moser, T.J. [2014]. Diffraction imaging of the Eagle Ford shale. *First Break*, **32**, 49-59.

Widess, M.B. [1973]. How thin is a thin bed?. *Geophysics*, **38** (6), 1176-1180.

Zaisheng, G., Zhu, W. and Zheng, B. [1994]. Reservoir and seal rock distribution and controlling factors in hydrocarbon-bearing rift basins of China, *AAPG International Conference and Exhibition*, Extended Abstracts.

Zavalishin, B. [1982]. Diffractions over deposit edges. *SEP Report* **32**, 137-147.

Zou, C. [2013]. *Volcanic Reservoirs in Petroleum Exploration*, Elsevier, The Netherlands.

Doi: 10.3997/1365-2397.2017006

ADVERTISEMENT

EAGE
EUROPEAN ASSOCIATION OF GEOSCIENTISTS & ENGINEERS

The National IOR Centre of Norway

University of Stavanger

IRIS IFE

Stavanger NORWAY

Register now!

Sustainable IOR in a Low Oil Price World

19TH EUROPEAN SYMPOSIUM ON IMPROVED OIL RECOVERY
STAVANGER, NORWAY | 24-27 APRIL 2017

Statoil